frontiers in Earth Science

ORIGINAL RESEARCH
published: 26 February 2021
doi: 10.3389/feart.2020.614267

The Role of Crystal Accumulation and Cumulate Remobilization in the Formation of Large Zoned Ignimbrites: Insights From the Aso-4 Caldera-forming Eruption, Kyushu, Japan

Franziska Keller[1]*, *Olivier Bachmann*[1], *Nobuo Geshi*[2] and *Ayumu Miyakawa*[2]

[1]Institute of Geochemistry and Petrology, ETH Zürich, Zürich, Switzerland, [2]Geological Survey of Japan (AIST), Tsukuba, Japan

The Aso-4 caldera-forming event (86.4 ± 1.1 ka, VEI-8) is the second largest volcanic eruption Earth experienced in the past 100 ka. The ignimbrite sheets produced during this event are some of the first ever described compositionally zoned pyroclastic flow deposits exhibiting clear compositional, mineralogical and thermal gradients with stratigraphic position. Large quantities of the deposits are composed of crystal-poor, highly evolved juvenile pumices, while late-erupted pyroclastic flows are in many cases dominated by crystal-rich and less silicic scoria. These petrological gradients in the Aso-4 deposits have been linked to extensive magma mixing of two compositionally distinct magmas in a complex upper crustal reservoir. However, new studies on several other zoned ignimbrites suggest that magma mixing alone is not sufficient to fully explain such strong compositional gradients in the deposits. These gradients are expected to be dominantly caused by the recharge-induced reactivation of extracted melt caps and their complementary cumulate in the upper crust. Here, we investigate bulk rock and matrix glass data with detailed analyses of mineral chemistry in order to re-evaluate the Aso-4 deposits in light of these latest developments. Reverse chemical zoning in phenocrysts, Sr enrichment in euhedral rims of plagioclase and the presence of mafic minerals (clinopyroxene, olivine) indicate recharge of hot, mafic magmas shortly prior to eruption, inducing a mixing signature. However, the marked enrichment in some elements in bulk-rock analyses and the presence of highly evolved minerals (some in the form of glomerocrysts) in the late-erupted, crystal-rich units, provide clear evidence for crystal accumulation in these scoria. Mass balance modeling of P_2O_5, Sr and SiO_2 supports the extraction of melt-rich lenses within an upper crustal mush zone, leaving a partly cumulative evolved crystal residue. We therefore propose an origin of the compositionally zoned Aso-4 ignimbrite largely by erupting a heterogeneous upper crustal reservoir, consisting of crystal-poor rhyodacitic melt caps within its associated cumulate mush. This complex reservoir was reactivated by mafic recharge shortly prior to eruption, imparting an additional mixing signature to the deposits.

Keywords: crystal accumulation, cumulate remobilization, ignimbrite, Aso caldera, silicic magma, magma mixing, magma chamber, super eruption

OPEN ACCESS

Edited by:
Michael Stock,
Trinity College Dublin, Ireland

Reviewed by:
Calvin Barnes,
Texas Tech University, United States
Victoria C Smith,
University of Oxford, United Kingdom

***Correspondence:**
Franziska Keller
franziska.keller@erdw.ethz.ch

Specialty section:
This article was submitted to Volcanology, a section of the journal Frontiers in Earth Science

Received: *05 October 2020*
Accepted: *24 December 2020*
Published: *26 February 2021*

Citation:
Keller F, Bachmann O, Geshi N and Miyakawa A (2021) The Role of Crystal Accumulation and Cumulate Remobilization in the Formation of Large Zoned Ignimbrites: Insights From the Aso-4 Caldera-forming Eruption, Kyushu, Japan. Front. Earth Sci. 8:614267. doi: 10.3389/feart.2020.614267

INTRODUCTION

Large-scale caldera-forming eruptions are typical examples of rare, but high-impact events, with major consequences on a local to global scale (Self, 2006; Self, 2015; Newhall et al., 2018; Papale and Marzocchi, 2019; De Maisonneuve and Bergal-Kuvikas, 2020; Geshi, 2020). They are commonly the result of the rapid evacuation of tens to thousands of cubic kilometers of silicic magmas typically stored in the upper curst (~2 ± 0.5 kb; Huber et al., 2019). The processes leading to the accumulation and evacuation of these enormous amounts of silicic magma in subvolcanic reservoirs are however complex and debated.

Typical volcanic products of large-scale caldera eruptions are "zoned ignimbrites", characterized by strong compositional, mineralogical and thermal gradients from early to late-erupted material. Those ignimbrites are usually produced by the rapid emptying of a complex, zoned magma reservoir in a single geological "instant" (i.e., on the order of days; Lipman, 1967; Wörner and Schmincke, 1984; Bacon and Druitt, 1988; Milner et al., 2003; Bachmann et al., 2014; Bachmann and Huber, 2016; Forni et al., 2016) and are interpreted to reflect reservoir conditions just prior to eruption. Hence, they offer the opportunity to evaluate pre-eruptive magma storage conditions prevailing immediately before the onset of catastrophic caldera-forming eruptions (Dunbar et al., 1989; Ellis and Wolff, 2012; Bachmann et al., 2014; Forni et al., 2016).

Existing models for the formation of such zoned magma reservoirs tend to cluster in two endmember scenarios.

(1) Models involving magma mixing of two or more compositionally distinct magma batches (Eichelberger et al., 2000; Hervig and Dunbar, 1992; Kaneko et al., 2007), or
(2) Models involving *in-situ* differentiation due to crystal-liquid separation in the subvolcanic magma reservoir (Lipman, 1967; Hildreth, 1981; Wörner and Schmincke, 1984; Bacon and Druitt, 1988; Wolff et al., 1999).

Recent studies, however, have suggested that both, *in-situ* differentiation and magma mixing, can play a significant role in the generation of such complex volcanic deposits (Bacon and Druitt, 1988; Hildreth, 2004; Deering et al., 2011; Pamukcu et al., 2013; Bachmann et al., 2014; Forni et al., 2016; Watts et al., 2016; D'Oriano et al., 2017; Foley et al., 2020). Efficient crystal-liquid separation at intermediate crystallinity (50–70%) from incrementally-growing mushy magma reservoirs is thought to produce melt-rich caps directly underlain by their complementary crystal-rich cumulates (Bachmann and Bergantz, 2004; Deering and Bachmann, 2010; Bachmann and Huber, 2016). This suggests the eruption of seemingly less differentiated cumulative portions of the reservoir (together with evidence of mafic recharge), following the eruption of crystal-poor, more evolved melt pockets (Bachmann and Bergantz, 2004; Deering et al., 2011; Bachmann et al., 2012; Bachmann et al., 2014; Evans and Bachmann, 2013; Pamukcu et al., 2013; Ellis et al., 2014; Wolff et al., 2015; Watts et al., 2016; D'Oriano et al., 2017; Foley et al., 2020), thus providing a working hypothesis for the generation of zoned ignimbrites.

This paper focuses on the understanding of one of the youngest, largest, and first-described cases of such a "supereruption", the Aso-4 caldera-forming event in Kyushu, southern Japan (Matsumoto, 1943; Lipman, 1967; Machida, 2002; Newhall et al., 2018; Takarada and Hoshizumi, 2020). Previous studies interpreted that extensive magma mixing of compositionally distinct magmas in a single upper crustal reservoir led to the formation of the observed gradients (Kaneko et al., 2007; Ishibashi et al., 2018). However, magma mixing alone is in many cases not sufficient to fully explain the strong compositional, mineralogical and thermal zonations in the pyroclastic deposits. Hence, we propose an updated model relating the origin of the voluminous Aso-4 ignimbrites to the formation of extracted silicic melt caps within a complementary cumulate mush, reactivated prior to eruption by less-differentiated recharge, inducing a faint but significant magma mixing signature.

Geological Background

The Aso caldera system is an archetypical example of an active, multicyclic caldera-forming volcanic edifice located in Central Kyushu, SW Japan (Machida and Arai, 1983; Hunter, 1998; Miyabuchi, 2009; Nobile et al., 2017; Tsuji et al., 2018; Albert et al., 2019). With a diameter of 18 × 25 km it is the second largest caldera system in Japan, formed by four devastating caldera-forming events (Aso-1 – 266 ± 14 ka, Aso-2 – 141 ± 5 ka, Aso-3 – 123 ± 6 ka, Aso-4 – 86.4 ± 1.1 ka) separated by extensive post- and pre-caldera activity from numerous central cones (Aoki, 2008; Miyabuchi, 2009, 2011; Miyoshi et al., 2012; Albert et al., 2019). Recent re-evaluations of the distribution and eruptive volumes of pyroclastic flow and tephra fall deposits in the Aso region revealed that the Aso-4 caldera-forming eruption is significantly larger in volume than previously estimated. With a total eruptive volume of 930–1860 km^3 (465–960 km^3 in dense rock equivalent) the event is now classified as a VEI 8 eruption (Volcanic Explosivity Index, Newhall and Self, 1982), representing the second largest volcanic eruption in the world in the past 100 ka (Takarada and Hoshizumi, 2020). Soon after the Aso-4 caldera-forming event, post-caldera activity from central cones resumed, producing relatively small volume eruptions of various compositions ranging from basalt to rhyolite (Miyabuchi, 2009; Miyabuchi, 2011; McLean et al., 2020).

The Aso-4 Eruption and Previous Hypotheses

The ignimbrite sheets produced during the Aso-4 eruption represent some of the first ever described zoned pyroclastic flow deposits ranging in bulk composition from basalt to rhyolite (Williams, 1942; Lipman, 1967; Hunter, 1998; Kaneko et al., 2007; Ishibashi et al., 2018). Lipman (1967) interpreted the zonation to reflect a single compositionally zoned magma chamber, which erupted in a short geological sequence. He

argued that the origin of the zoned ignimbrite sheets might be caused by a combination of different scenarios, including 1) mixing of two compositionally distinct magmas in the subsurface, 2) differentiation (including potential crystal fractionation and/or anatectic melting) in a large "continuous" magma reservoir underlying the erupted portion or 3) differentiation by vertical volatile transfer.

In 2007, Kaneko *et al.* conducted a detailed petrographic study of the eruptive products to examine the pre-eruptive magma chamber configuration of the Aso-4 event. They divided the eruptive sequence in two distinct subcycles separated by a sharp boundary, with each subcycle being characterized by a progression from silicic to mafic magmas. The observed zonations within the first subcycle were explained by a pre-eruptive magma chamber setup comprising a silicic magma layer at the top of the reservoir and a mafic magma layer at the bottom of the reservoir, showing gradual decrease of SiO_2 with increasing depth. Magma mixing of the silicic endmember magma and the upper, most silicic part of the mafic layer is interpreted to have formed a hybrid magma layer in between the two endmember magmas (Kaneko et al., 2007). During the first subcycle, extensive magma mixing of the silicic magma, the first hybrid magma and the upper part of the mafic magma layer led to the formation of a second hybrid magma within the reservoir. After a short repose, the eruption of the second subcycle began with the emptying of the second hybrid magma and ended with the discharge of mafic scoria petrologically similar to the mafic magma in subcycle one. Thus, magma mixing in a single, large upper crustal reservoir is interpreted to be the main factor initiating the observed gradients in the Aso-4 deposits.

Following the conclusions of Kaneko et al., (2007), Ishibashi et al., (2018) quantified composition-temperature-pressure conditions of the silicic endmember magma based on single-phase amphibole chemistry. They concluded that amphiboles, even though euhedrally-shaped, were in chemical and thermal disequilibrium with high-silica host melt and thus mostly crystallized from a locally separated hydrous melt comprising 63–69 wt% SiO_2 at 910–950°C. Based on these findings, they gave new constraints on the structure of the pre-eruptive system comprising a silicic melt layer as described by Kaneko et al., (2007) underlain by three distinct layers of crystal mush. Those mush layers were interpreted to have varying mineral assemblage, where one locally limited, volatile-rich mush layer was thought to contain amphiboles. Just prior to eruption, disruption of the crystal mush (the "partial collapse" of Ishibashi et al., 2018) was triggered by the intrusion of mafic magma from underneath, leading to the incorporation of amphibole crystals into the silicic melt layer at the top of the reservoir (Ishibashi et al., 2018). Observed chemical and crystal gradients within the Aso-4 deposits, were interpreted to be primarily formed by magma mixing following the interpretations of Kaneko et al., (2007). Pre-eruptive P-T conditions of the silicic endmember magma of the Aso-4 reservoir were determined by Ushioda et al., (2020) based on high P-T experiments yielding temperatures around 900 °C, pressures of ≤300 MPa and water contents ≤3 wt% H_2O.

Despite the clear evidence of magma mixing within the Aso-4 system, this hypothesis cannot entirely explain the observed zonations and associated mineral compositions found in the Aso-4 deposits. For example, homogeneous groundmass glass and strontium isotopic ratios observed in silicic as well as mafic Aso-4 units suggest a genetic relation between the different units rather than being formed independently (Hunter, 1998; Kaneko et al., 2007; Wolff et al., 2015; Forni et al., 2016). Furthermore, magma mixing is, when occurring in large quantities as suggested by Kaneko et al., (2007), interpreted to strongly affect the bulk rock chemistry of the subvolcanic system. However, it fails to reproduce the strong crystallinity gradients and typically homogeneous and evolved mineral compositions that characterize the Aso-4 ignimbrite sheets (Kaneko et al., 2007). Based on these observations, re-evaluation of bulk rock, groundmass glass and mineral chemistry were performed in order to test the previous hypotheses in light of the latest findings on the generation of zoned ignimbrites.

METHODS

Sampling

A total of 8 different samples were collected from 6 sampling sites around the center of Aso caldera (**Figure 1**). Fresh, juvenile clasts were sampled at different stratigraphic heights from, among others, the 4I-1 (non-welded pumice flow), 4I-3 (non-to weakly-welded scoria flow with small amounts of pumice and banded pumice) and 4II-2 (densely-welded silicic pyroclastic flow) units described in Kaneko et al., (2007), (see **Supplementary Table S1**).

Bulk-Rock Major Element Compositions

Major element bulk rock compositions were analyzed via X-ray fluorescence (XRF) spectrometry at the Geological Survey of Japan (GSJ), AIST, Tsukuba applying a glass-bead method. Fresh, juvenile pumice clasts were cleaned, powdered and mixed with Tetraborate dilithium powder with a dilution ratio of 1:10 of sample against the flux.

Matrix Glass and Mineral Compositions

In order to reduce beam damage during matrix glass analysis, measurements were conducted by using an EDS-calibrated JEOL JSM-6390 LA Scanning Electron Microscope (SEM), equipped with a Thermo Fisher NORAN NSS7 EDS system with LaB6 filament, 30 mm^2 silicon-drift detector and Faraday-cup for calibration. This method allows averaging measurements over wide areas (average diameters of 25 μm). To monitor the accuracy of the measurements, glasses, which were analyzed via electron probe micro analyzer (EPMA), were used as secondary standards (EDS calibrated SEM and EPMA analyses can be found in

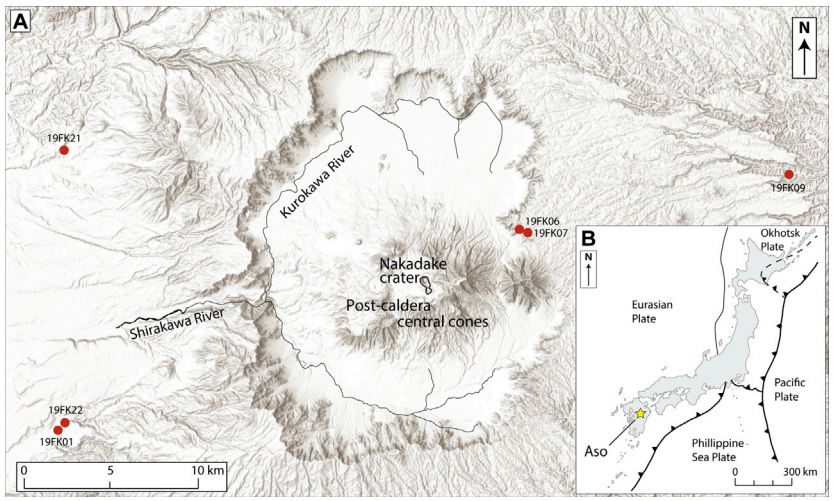

FIGURE 1 | (A) Location map of the sampling sites around Aso Caldera. The relief map was produced with the online ArcGIS viewer (https://www.arcgis.com/home/webmap/viewer.html). **(B)** Location of Aso caldera (yellow star) in central Kyushu. Black lines indicate plate boundaries with triangles marking the sense of subduction.

Supplementary Table S1). A detailed description of the method can be found in (Popa et al., 2019).

Mineral major element compositions were measured from hand-picked minerals mounted in epoxy via EPMA at ETH Zuerich. Operating conditions were set to 15 kV acceleration voltage, 20 nA beam current and counting times of 20 s on the peaks and 10 s on the background. To minimize alkali loss, a defocused beam with a spot size of 10 µm was used for plagioclase and amphibole measurements.

Trace element concentration in mineral phases and matrix glasses were analyzed using a 193 nm Resonetics Resolution 155 excimer laser ablation system coupled to a Thermo Element XR sector field mass spectrometer at ETH Zuerich. A spot size of 29 µm was used for pyroxene analysis while a spot size of 43 µm was used for plagioclase and amphibole measurements. Spot sizes of 19 and 29 µm were alternately used for matrix glasses depending on the porosity of the sample. The softwares SILLS (Guillong et al., 2008) and IOLITE 4 (Paton et al., 2011) were used for data reduction using NIST 610 and NIST 612 as primary standards and GSD-1G as secondary standard to monitor the accuracy of the measurements. SiO_2 contents from preceding EPMA and SEM measurements were used as internal standards for mineral phases and matrix glasses (calibrated trace element analysis can be found in **Supplementary Table S2**).

Relative Crystallinity

Crystallinity of 8 samples was determined by X-ray powder diffraction (XRD) using an AXS D8 Advance diffractometer equipped with a Lynxeye super speed detector at ETH Zuerich following the method of Rowe et al., (2012). Powdered samples were analyzed using CuKα radiations generated at 40 kV and 40 mA applying the following settings: 5°–90° (2θ scan interval), 0.02° step size, 2 s time/step and V12 divergence and anti-scattering slits. A calibration curve based on glasses containing known crystal contents (Forni et al., 2016) was used to determine the porphyritic index.

RESULTS

Bulk Rock and Matrix Glass Compositions

New bulk rock data are combined with literature data from Kaneko et al., (2007) in order to obtain a complete overview of the bulk compositional variability of Aso-4 products. Observed trends follow a typical high-potassium, calc-alkaline trend ranging from basalt to rhyolite (**Supplementary Figure S1**). A compositional gap is found between SiO_2 concentrations of 57 wt% to 63 wt%, implying a dearth of andesitic material in the erupted products (**Figures 2A–C**). Early-erupted clasts exhibit silicic bulk compositions, while late-erupted scoria are of typically more mafic bulk composition than the early-erupted pumices (**Figures 2A–C**). When being compared to average basaltic compositions (Kelemen et al., 2003), crystal-rich scoria show a clear divergence due to pronounced enrichment of some elements (compatible in specific mineral phases, see below) in Aso-4 mafic clasts (**Figures 2A–C**). Crystallinity measured for late-erupted scoria varies between ~45% to 55% while early-erupted, silicic clasts are found to have significantly lower crystallinities between ~5%–25% (**Figure 3**, **Supplementary Figure S2**).

Major element matrix glass compositions from early and late-erupted clasts overlap in a compositional range between 68 wt% to 75 wt% SiO_2 (**Figures 2A,B**). However, less evolved compositions (≤68 wt% SiO_2) are also found but exclusively in late-erupted, crystal-rich units. Trace elements in matrix glasses overlap likewise but are generally more variable. Zr concentrations are typically low, in agreement with the lack of zircon in the deposits (**Figures 2D–F**). Eu anomalies are

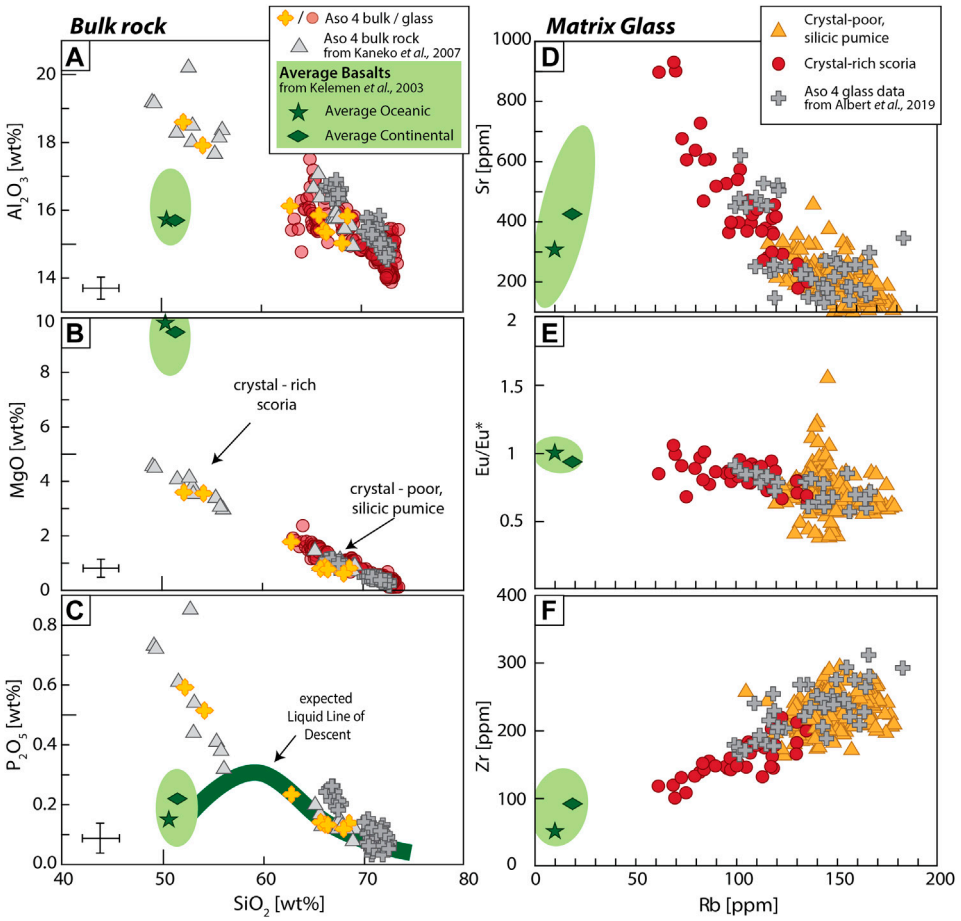

FIGURE 2 | Geochemical overview of Aso-4 bulk rock and matrix glass compositions. Colored symbols refer to data from this study, while gray triangles and crosses represent literature data from Kaneko et al., (2007) and Albert et al., (2019), respectively. Bulk rock major elements **(A)** Al_2O_3, **(B)** MgO and **(C)** P_2O_5 are plotted vs. SiO_2 showing a compositional gap between SiO_2 concentrations of 57–63 wt%. Matrix glass trace elements **(D)** Sr, **(E)** Eu/Eu* (Eu* = $Eu_N/(Sm_N{}^*Gd_N)^{1/2}$) and **(F)** Zr are plotted vs. Rb showing partial overlap between matrix glasses from crystal-poor pumices and crystal-rich scoria. Light green areas mark average basaltic compositions taken from literature (Kelemen et al., 2003) showing a pronounced shift of crystal-rich scoria to average basaltic compositions. Error bars given in **(A)**–**(C)** refer to errors of whole rock data from this study, errors of matrix glass measurements are smaller than the symbol.

generally slightly negative; only a single sub-unit (19FK07; a silicic, crystal-poor welded ignimbrite included in the early-erupted units) shows pronounced variability in Eu anomaly from deeply negative to a clearly positive anomaly (**Figure 2E**).

Mineral Assemblage

Early-erupted, crystal-poor and late-erupted, crystal-rich units comprise identical mineral assemblages consisting of plagioclase, ortho- and clinopyroxene, amphibole, Fe-Ti oxides (magnetite and ilmenite), and apatite (±olivine). Zircon is not found in any parts of the ignimbrites, despite intensive search and being close to zircon saturation at 775°C (Watson and Harrison, 1983; Boehnke et al., 2013). Phenocrysts are usually large in size (>>0.5 mm; Kaneko et al., 2007, **Supplementary Figure S2**) and groundmass microlites are only rarely found in individual crystal-rich clasts.

Pyroxenes

Ortho- and clinopyroxene are present in all investigated Aso-4 samples with orthopyroxene generally more abundant than clinopyroxene. Clinopyroxene is of augitic to diopsidic composition (**Supplementary Figure S3**) and euhedral to subhedral shape with rare resorbed rims (**Figure 4B**). Various zonation patterns are present, ranging from completely unzoned to complexly zoned crystals, some of which contain orthopyroxene cores. Complex zoning patterns are predominantly found in grains from late-erupted, crystal-rich clasts (**Figure 4B**). Clinopyroxene in early-erupted, silicic pumices and late-erupted scoria overlap within a narrow compositional range of Mg numbers (between 71 to 83 (Mg# = Mg/(Mg + Fe)*100; **Figure 4B**) compared to other arc volcano systems (e.g., Methana, Greece Mg# = 50–85, Popa et al., 2020). Mafic clinopyroxene is characterized based on high Mg# and high Cr content and is present in both silicic pumices as well as mafic scoria (**Figure 4A**). REE patterns do

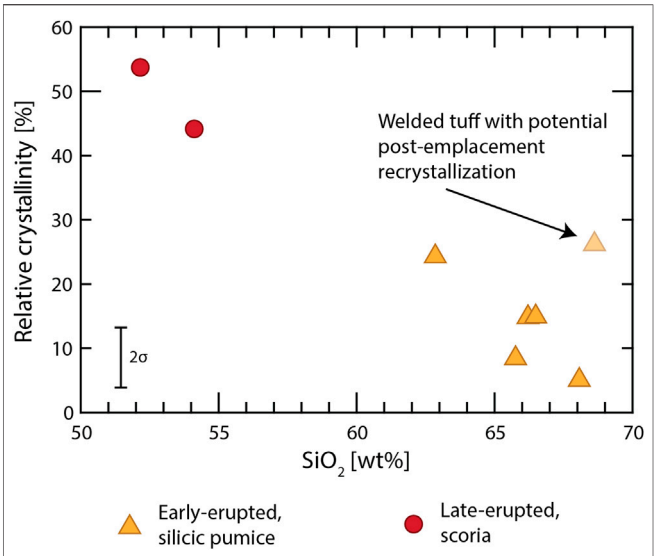

FIGURE 3 | Plot of bulk SiO_2 content vs. crystallinity of early-erupted, silicic pumices and late-erupted scoria. Crystallinity in early-erupted pumices is markedly lower than in late-erupted scoria.

not distinguish between crystals from early-erupted, crystal-poor and late-erupted, crystal-rich units. Generally, REE concentrations are high, comparable to concentrations found in grains originating from silicic units, indicating crystallization from evolved melts (**Figure 4C**).

Orthopyroxene is euhedral to subhedral, with numerous inclusions of plagioclase, Fe-Ti oxides, apatite and melt. Compositional zonation of orthopyroxene is usually weak and if present predominantly found in grains from late-erupted, crystal-rich units. Similar to clinopyroxene, major as well as trace element composition for crystals from late-erupted scoria and early-erupted, silicic units overlap in composition, implying crystallization from similarly evolved melts in a narrow compositional range (Mg# = 71–77; **Figures 4C,D**) compared to other arc volcano systems (e.g., Methana, Greece, Mg# = 45–70, Popa et al., 2020).

Plagioclase

Plagioclase is the most abundant mineral in Aso-4 deposits, reaching modal contents of up to 25 vol% (Kaneko et al., 2007). In early-erupted, silicic pumices plagioclase is typically euhedral and often unzoned (**Supplementary Figure S2**). However, multiple zoned grains can be found, exhibiting various zoning patterns including oscillatory, normal, and patchy zoning. In late-erupted, crystal-rich scoria, plagioclase typically has a sieved structure, sometimes overgrown by rims of intermediate An-content ($An_{50–60}$, **Figure 5C**). The plagioclase from late-erupted scoria is usually strongly zoned, frequently showing oscillatory, patchy, and normal zoning patterns. A compositional overlap between crystals from silicic pumices and crystal-rich scoria is observed between An-contents of 30%–75%. However, grains from crystal-rich scoria tend to expand to more calcic compositions than in silicic pumices (**Figure 5A**). Likewise, SrO concentrations measured in

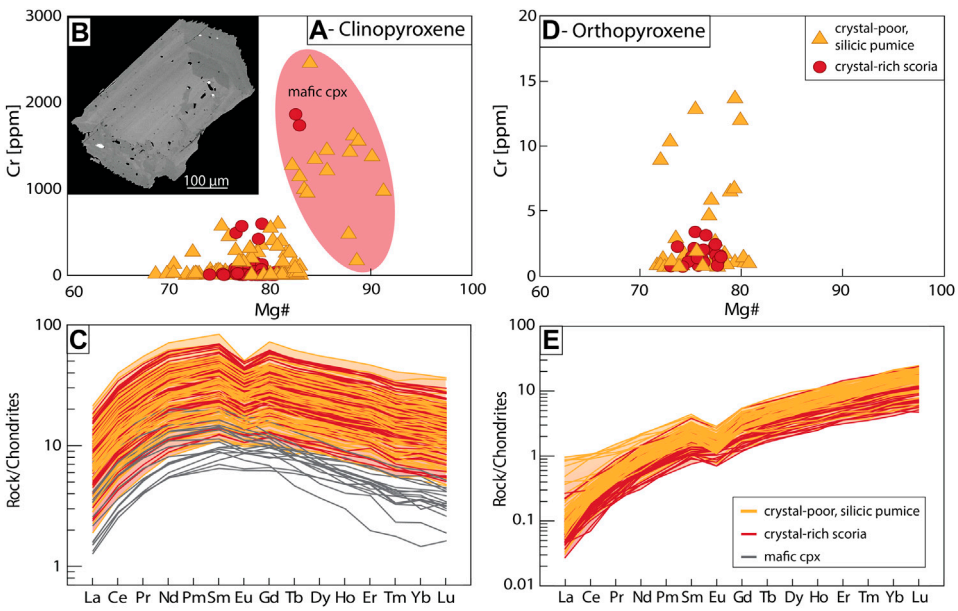

FIGURE 4 | Compositional variations of clino- **(A)**–**(C)** and orthopyroxene **(D)**, **(E)** from crystal-poor, silicic pumice and crystal-rich scoria. **(A)** Binary plots of Cr vs. Mg# [Mg# = Mg/(Fe + Mg) × 100)] indicate the presence of mafic clinopyroxene with high Mg# and high Cr in both, early-erupted pumices and late-erupted scoria. **(D)** Orthopyroxene shows a less pronounced spread of Cr at distinctly lower concentrations than clinopyroxene implying crystallization from slightly more evolved melts. REE patterns of clinopyroxene **(C)** do not distinguish silicic pumices from scoria but give lower REE contents for mafic scoria. Orthopyroxene REE patterns **(E)** plot in a narrower compositional range than clinopyroxene suggesting crystallization from compositionally less variable melts. Measurement errors are smaller than the symbol.

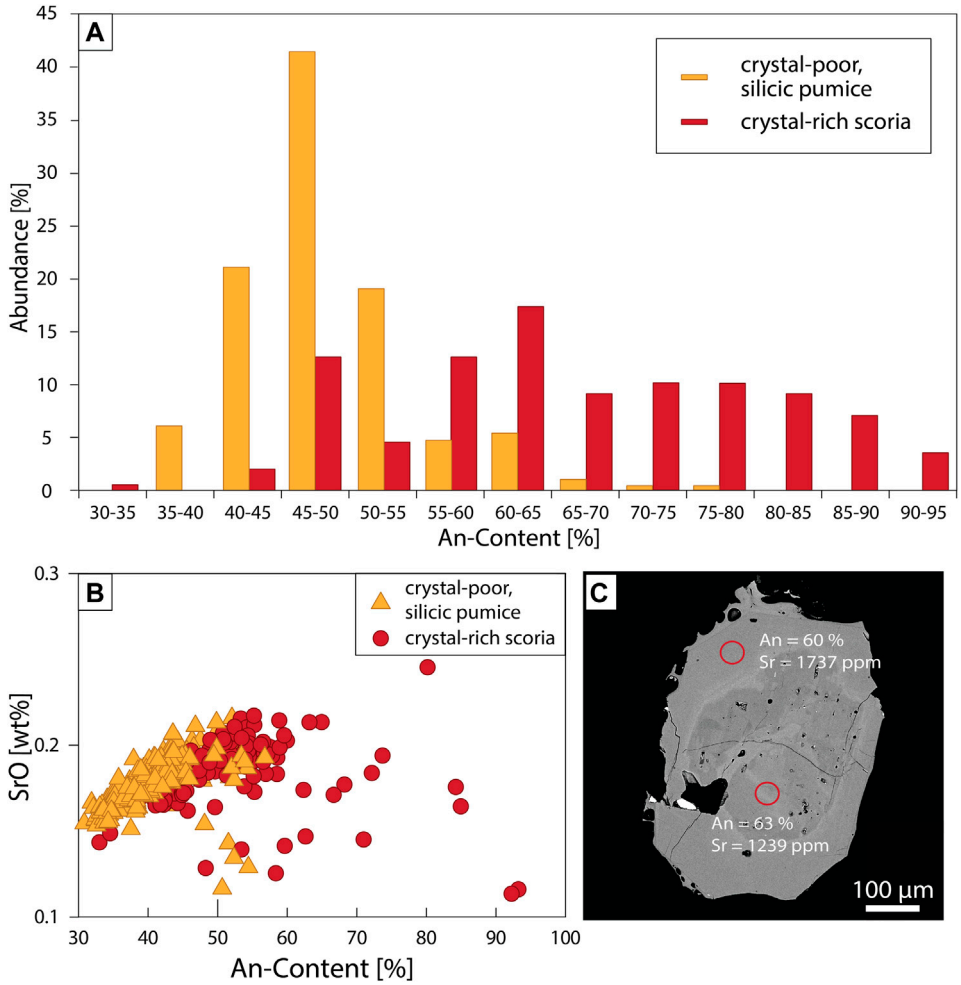

FIGURE 5 | Geochemical overview of Aso-4 plagioclases from crystal-rich scoria and crystal-poor, silicic pumice. **(A)** Histogram of An-contents of Aso-4 plagioclase. An contents for plagioclases overlap in the range of $An_{30–75}$; early-erupted plagioclases tend to cluster around lower An contents while plagioclases from late-erupted units tend to shift toward higher An contents. Crystals with An > 75 are identified as recharge crystals based on test for equilibrium (following Putirka, 2016). **(B)** Binary plot of SrO vs. An-content displaying compositional overlap of plagioclase from early-erupted pumice and late-erupted scoria, with a tendency toward more mafic compositions in plagioclase from crystal-rich scoria. **(C)** Backscattered image of a plagioclase from late-erupted scoria exhibiting a sieved texture core overgrown by an euhedral rim of An_{60} and clear Sr enrichment within the crystal rim. Measurement errors are smaller than the symbol.

plagioclase from the different units show a broad compositional overlap between $An_{30–60}$, where grains from late-erupted units slightly shift toward more calcic compositions than early-erupted ones (**Figure 5B**). Euhedral crystal rims of sieved plagioclases from late-erupted, crystal-rich scoria, sometimes exhibit notable Sr enrichment compared to sieved crystal cores (**Figure 5C**).

Amphibole

Amphibole in the Aso-4 units is euhedral to subhedral (**Figure 6B**) and most individual crystals show little to no chemical zoning, although compositional variations are observed between individual grains. The compositional variations in Aso-4 amphibole is relatively narrow compared to the compositional spread recognized in other dacitic arc volcanoes (e.g., Mt. St. Helens, USA (Humphreys et al., 2019), Ciomadul, Romania (Kiss et al., 2014); **Figure 6A**). However, similarly chemically restricted amphibole compositions were found in other large zoned ignimbrites like the Carpenter Ridge Tuff, USA, implying amphibole crystallization in such extensive systems from chemically less variable melts (Bachmann et al., 2014, **Figures 6A,E**). Furthermore, no compositional variations are found between amphibole from early-erupted and late-erupted clasts, similar to the observations from pyroxenes and plagioclase (**Figures 6A–C,E**). High REE contents in Aso-4 amphibole (**Figure 6F**) imply crystallization from evolved melts, with crystals from silicic clasts being indistinguishable from grains from crystal-rich scoria. Eu anomalies of Aso amphibole increase with increasing Si, indicating growing influence of plagioclase co-crystallization with melt evolution. When zoned, amphibole reveals core-to-rim profiles with two different characteristics: 1) rimward increase of Al^{IV}, $(Na + K)^{A}$ and Al^{VI} concomitant with decrease of SiO_2, Ti and Mn

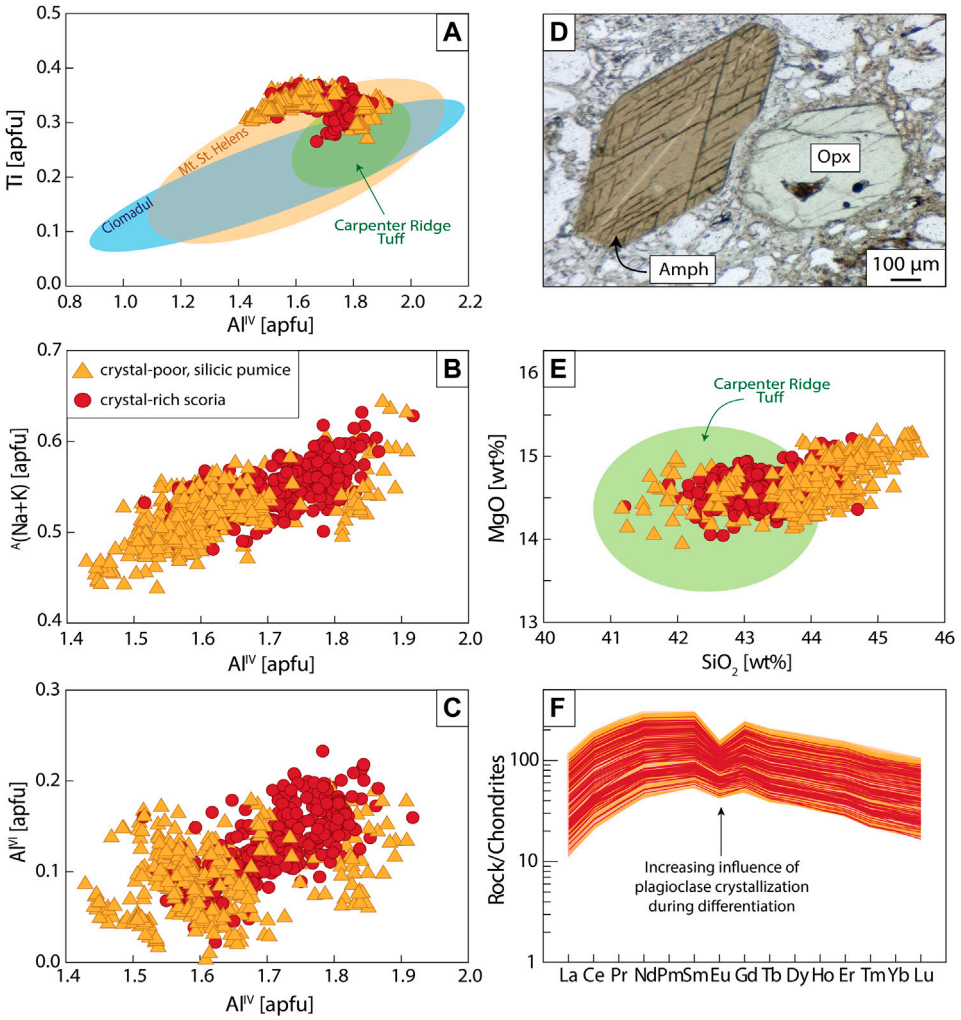

FIGURE 6 | Amphibole composition in silicic, crystal-poor pumice and crystal-rich scoria. Binary plots of **(A)** Ti, **(B)** ^{A}(Na + K) and **(C)** Al^{VI} vs. Al^{IV} illustrate substitution conditions in Aso-4 amphibole. Comparisons to amphiboles from Mount St. Helens (orange fields, Humphreys et al., 2019), Ciomadul (blue fields, Kiss et al., 2014) and Carpenter Ridge Tuff (green fields, Bachmann et al., 2014; Lipman, 2006) indicate high homogeneity in Aso-4 amphiboles similar to CRT samples. **(D)** Photomicrograph of a late-erupted, euhedral amphibole from crystal-rich scoria together with orthopyroxene. **(E)** Plot of MgO vs. SiO_2 comparing Aso-4 amphibole to CRT amphiboles. **(F)** Chondrite-normalized (Sun and McDonough, 1989) REE patterns of Aso-4 amphiboles show a range of REE compositions. Eu anomaly is progressively increasing with ongoing melt differentiation due to increasing influence of plagioclase crystallization. Measurement errors are smaller than the symbol.

(measured in about one third of the investigated grains, **Figure 7A**), 2) Recurring troughs of Al^{IV}, $(Na + K)^{A}$ and Al^{VI} recognized in some grains (**Figure 7B**), which suggest variable reservoir conditions during amphibole crystallization (see discussion).

DISCUSSION

Our new data confirm the previously-described strong compositional and mineralogical gradients in the Aso-4 deposits (since Lipman, 1967). Kaneko et al., (2007) and Ishibashi et al., (2018) agreed that magma mixing in a single, large reservoir is mostly responsible for the formation of the observed features. However, as mentioned above, a couple of petrological observations suggest that magma mixing alone is not sufficient to produce these strong zonations, as also pointed out for several other zoned ignimbrites (e.g., Mount Mazama, Bacon and Druitt, 1988; Ammonia Tanks Tuff, Deering et al., 2011; Carpenter Ridge Tuff, Bachmann et al., 2014; Wolff et al., 2015; Campi Flegrei, Forni et al., 2016);

1. Homogeneous groundmass glass compositions and Sr isotopic ratios among the different units imply a clear genetic relation between the units.
2. Partially overlapping mineral compositions in silicic and mafic clasts in a narrow compositional range is in contradiction with the wide compositional range observed for bulk-rock analysis.

Hence, in the following section, we examine the applicability and potential extension of recent models from

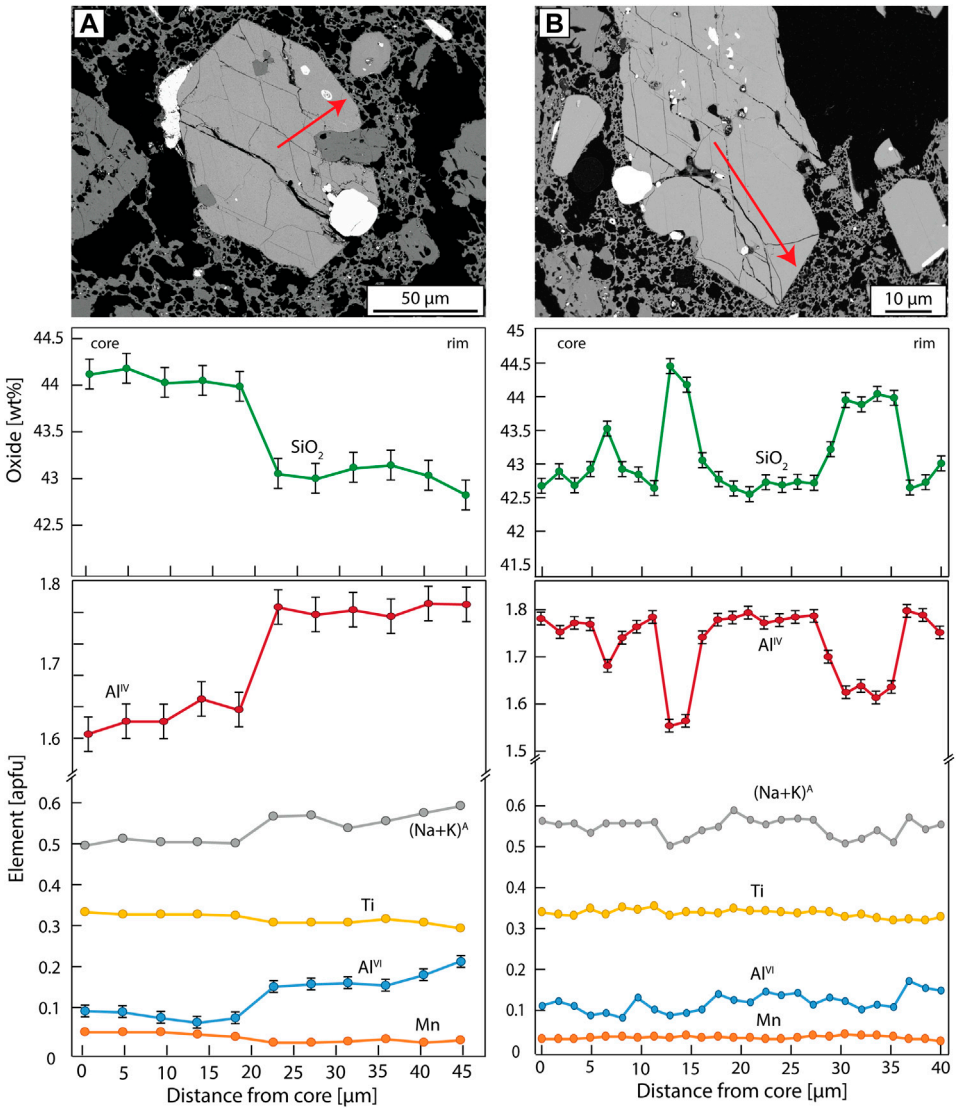

FIGURE 7 | Core-to-rim concentration profiles of Aso-4 amphibole. Profile trajectories are indicated by red arrows in back-scattered images. **(A)** shows the most common zoning pattern of Aso-4 amphibole (present in about one third of the measured amphiboles) displaying increasing Al^{IV}, $(Na + K)^{A}$ and Al^{VI} concomitant with decreasing SiO_2, Ti and Mn toward the rim indicating increasing reservoir temperature during crystallization. Changes might also be influenced by changing pressure and melt composition. **(B)** shows an oscillatory zoned amphibole with recurring Al^{IV}, $(Na + K)^{A}$ and Al^{VI} troughs suggesting cyclic reheating/recharging of the reservoir during amphibole fractionation. Where not given errors are smaller than the symbol.

previous studies to the Aso-4 system, linking the formation of zoned ignimbrites to melt extraction in an extensive upper crustal cumulate mush (Bachmann and Bergantz, 2004; Deering et al., 2011; Bachmann et al., 2012, 2014; Evans and Bachmann, 2013; Pamukcu et al., 2013; Ellis et al., 2014; Wolff et al., 2015; Watts et al., 2016; D'Oriano et al., 2017; Foley et al., 2020).

Equilibrium Assemblage

In order to estimate pre-eruptive magma conditions in different parts of the Aso-4 reservoir, we subdivided the reservoir into three potentially different sections (silicic cap, cumulate mush and recharge following previous models) based on matrix glass chemistry. A silicic cap endmember in this case is interpreted to be (rhyo-)dacitic in composition, reflecting matrix glass compositions found in both crystal-poor pumices and crystal-rich scoria. A cumulate mush endmember consists of mildly less differentiated matrix glass composition than the silicic cap, represented by dacitic melt compositions found in crystal-rich scoria. The transition between the silicic cap endmember and the cumulate mush endmember, however, is assumed to be gradual due to the influence of potential recharge-induced mixing. Melt inclusions in mafic clinopyroxene (high Mg# and Cr) are of andesitic-dacitic melt composition, which is not present in any of

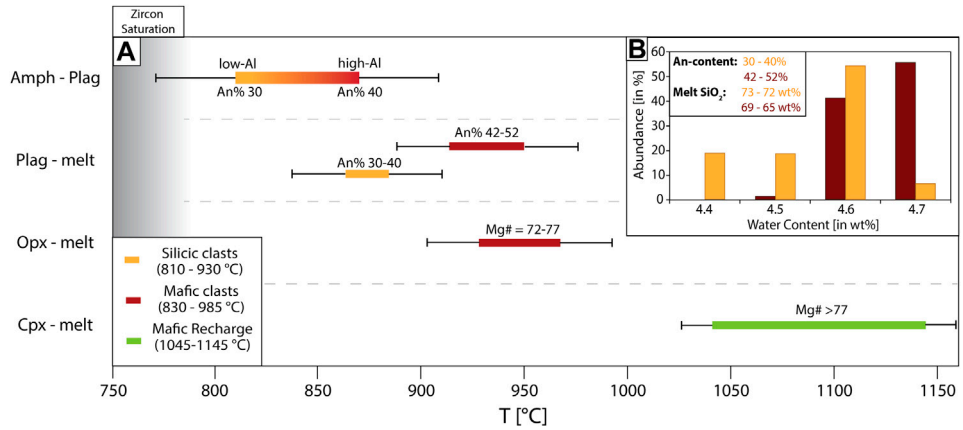

FIGURE 8 | Pre-eruptive temperatures **(A)** and water contents **(B)** for three different Aso equilibrium assemblages. Orange colors display mineral assemblages in equilibrium with (rhyo-)dacitic melt, red colors indicate equilibrium with dacitic melt present in the cumulate mush and green stands for assemblages in equilibrium with mafic recharge melt. Temperatures were calculated applying different thermometers. The length of the bars indicate the range of temperatures obtained by each thermometer, black extensions show the range of errors. The Amph-Plag thermometer is the plagioclase-amphibole thermometer (Holland and Blundy, 1994) and the Plag-melt, Opx-melt and Cpx-melt thermometers stand for plagioclase- and pyroxene-melt thermometers from Putirka (2016, 2008). Summarized temperature ranges for each equilibrium assemblage are given in the lower left corner. Water contents in **(B)** are calculated for plagioclases in equilibrium with (rhyo-)dacitic and dacitic melt, independently, applying the hygrometer from Waters and Lange (2015).

the investigated pumice or scoria samples, but implies the presence of less differentiated recharge melts (available melt inclusion data is given in **Supplementary Table S1**). Based on this subdivision, mineral-melt equilibrium tests were conducted applying the tests of Putirka (2008, 2016), Zhang et al., (2017), and Humphreys et al., (2019) revealing the following mineral-melt equilibrium assemblages (**Supplementary Figure S4**):

(1) (Rhyo-)Dacitic cap: low-Al amphibole ($Al^{IV} \leq 1.6$ apfu), low-An plagioclase ($An_{\leq 35}$), with abundant apatite, ilmenite and magnetite found as inclusions in those minerals.
(2) Dacitic cumulate mush: high-Al amphibole ($Al^{IV} \geq 1.7$ apfu), intermediate to high-An plagioclase (An_{40-70}), orthopyroxene, clinopyroxene (Mg# ≤ 80), and abundant apatite, ilmenite and magnetite present as inclusions in many crystals.
(3) Intermediate recharge: clinopyroxene (Mg# ≥ 85), high-An plagioclase ($An_{<70}$), rare olivine.

Pre-Eruptive Magma Conditions

Based on the mineral-melt equilibrium pairs described in the previous section, we calculated temperature, pressure and dissolved water contents for a (rhyo-)dacitic melt cap, a cumulate mush and intermediate recharge, independently.

Temperature Conditions

Temperatures of the reservoir were estimated using a variety of different thermometers, including (i) amphibole-plagioclase pairs (Holland and Blundy, 1994), (ii) plagioclase-melt equilibrium pairs (Putirka, 2016) and (iii) ortho- and clinopyroxene - melt equilibrium pairs (Putirka, 2008).

Temperature estimates for a possible (rhyo-)dacitic melt cap at the top of the reservoir range from 810 to 930°C (±40°C) (**Figure 8A**). Corresponding temperatures for a cumulate mush broadly overlap with the temperatures obtained for the (rhyo-)dacitic melt cap, but extend toward higher temperatures in a range between 830–985 °C (±40 °C). Clinopyroxene–melt thermometry for andesitic-dacitic recharge melt revealed temperatures of up to 1050–1150 °C (±25°C).

Pressure Conditions

Pre-eruptive reservoir pressures were calculated applying the Al-in-hornblende barometer of Anderson and Smith (1995). Calculated pressures vary around approximately 2 kbar for both (rhyo-)dacitic melt cap and cumulate mush. The pressures calculated for amphiboles crystallized from (rhyo-)dacitic melt tend to show slightly lower pressures than amphiboles crystallized from a dacitic melt.

Pre-eruptive Water Contents

In order to estimate pre-eruptive magmatic water contents in the reservoir (and potentially check for gradients), the plagioclase-liquid hygrometer of Waters and Lange (2015) was applied for equilibrium pairs of (rhyo-)dacitic and intermediate melt using plagioclase of An_{30-35} and An_{40-50} to reflect the melt cap and cumulate mush, independently (**Figure 8B**). The calculated magmatic water contents for melt cap and cumulate mush overlap within error varying in the range of 4.4–4.7 wt% (±0.35 wt%).

Indications for Cumulate Formation and Pre-eruptive Remobilization

Indications for crystal accumulation in the erupted products of Aso-4 can be derived from various lines of evidence, as outlined in the following section.

Evidence From the Geochemical Record

Mineral compositions in the Aso-4 clasts are compositionally restricted over the full stratigraphic range and show extensive

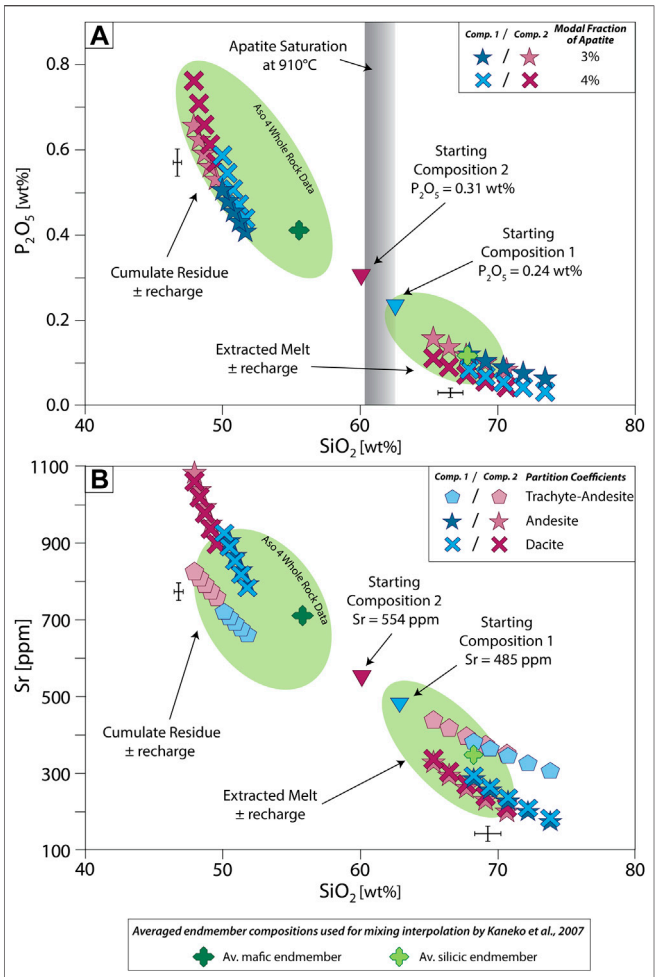

FIGURE 9 | Major and trace element modeling using **(A)** P_2O_5 and **(B)** Sr vs. SiO_2 based on Rayleigh fractionation. Starting compositions of two natural samples of intermediate composition (1 = blue, 2 = purple) are marked as triangles. Modal proportions used to calculate bulk partition coefficients applied in the model calculations were given in Kaneko et al., (2007). However, in P_2O_5 models **(A)** modal fractions for apatite were varied between 3% and 4%. In Sr models **(B)** partition coefficients for Sr in plagioclase were varied for different melt compositions. Green fields illustrate Aso-4 whole rock data, green symbols represent the endmembers used for mixing modulations in Kaneko et al., (2007). Error bars indicate the 2σ error of the respective modeled element concentrations.

overlap between silicic and more mafic units (**Figures 4–6**). These findings indicate that crystals in nearly all Aso-4 products crystallized from similarly evolved melts of dacitic to (rhyo-) dacitic compositions. The difference in crystallinity, and in bulk-rock composition is therefore largely due to the physical accumulation of crystals (or more accurately of melt loss). Pooling of those melts led to the formation of a melt-rich silicic cap in the upper parts of the reservoir, leaving complementary crystal-rich zones with a cumulate signature in the deeper parts of the reservoir (Deering and Bachmann, 2010; Wolff et al., 2015, 2020). Textural evidence for such crystal accumulations, however, is often only barely preserved in the eruptive products. Magmatic foliation or crystal clusters, which are common textural tracers for crystal accumulation in silicic plutons (e.g., Žák et al., 2007; Beane and Wiebe, 2012; Graeter et al., 2015; Barnes et al., 2016; Fiedrich et al., 2017), are disrupted by the dynamic processes taking place within the reservoir and during the turbulent ascent of the magma through the conduit (Meurer and Boudreau, 1998; Ellis et al., 2014; Fiedrich et al., 2017). Nevertheless, evidence for crystal packing at the edges of the Aso-4 magma reservoir initiated by melt extraction is given by the presence of glomerocrysts as described by Kaneko et al., 2007 (see also Ellis et al., 2014; Bachmann and Huber, 2019; Holness et al., 2019, Lubbers et al., 2020).

Evidence From Mass Balance Modeling

In order to test the hypothesis of cumulate formation in the Aso-4 system, element modeling of P_2O_5, Sr and SiO_2 concentrations was performed (**Figure 9**, following Deering and Bachmann (2010), Gelman et al., (2014), and Forni et al., (2016), see **Supplementary Table S3**). P_2O_5 was selected based on its distinct behavior during magma differentiation (see Lee and Bachmann, 2014): until apatite saturation, P_2O_5 behaves incompatibly, however, as soon as apatite begins to crystallize, P_2O_5 becomes strongly compatible in apatite, developing a prominent kink in the liquid line of descent (**Figure 2C**). This behavior classifies P_2O_5 as an optimal element to distinguish between low-SiO_2 cumulate residue and basaltic liquids. Sr can also be useful, as it is strongly compatible in plagioclase, the most common mineral phase in Aso samples, and thus likely shows enrichment in plagioclase accumulation zones. In both cases, a clear discrepancy between Aso bulk rock compositions and average basaltic compositions is seen, outlining P_2O_5 and Sr enrichment in Aso-4 scoria (**Figures 2C,D**).

Rayleigh fractionation equations (Rollinson, 1993; Deering and Bachmann, 2010) were used to independently calculate P_2O_5 and Sr concentrations in potential extracted melts and residual cumulate, that were subsequently compared to Aso-4 bulk rock compositions. Starting compositions, from which extracted melt and residual cumulate compositions were calculated, were taken from two different natural samples of intermediate composition, assuming the initial magma was not of primitive composition but already more evolved due to pre-conditioning in lower crustal reservoirs (**Figure 9**). Modal proportions given in Kaneko et al., (2007) were used to calculate bulk partition coefficients applied in the models following the approach of Rollinson (1993). Apatite modal amounts for the P_2O_5 models were estimated to vary between 3% and 4% (**Figure 9A**). Appropriate partition coefficients (K_D) used to calculate the bulk partition coefficients were selected from the GERM database (https://earthref.org/KDD/), choosing variable K_D of Sr in plagioclase depending on melt composition (trachy-andesite, andesite and dacite) in Sr calculations (**Figure 9B**).

The modeled element concentrations clearly coincide with the observed Aso-4 compositions reproducing a high Sr-P_2O_5, low-SiO_2 cumulate residue overlapping with crystal-rich Aso-4 scoria. Extracted melts, high in SiO_2 and low in Sr and P_2O_5, on the other hand, clearly coincide with the crystal-poor pumices. Small discrepancies between the model results and observed element

compositions can be induced by the involvement of some mafic recharge or limited crustal assimilation during magma evolution.

Eu anomaly is usually also a commonly-used indicator for tracing cumulate signatures in whole rock samples. A positive Eu anomaly is typically thought to mark the accumulation of plagioclase in a cumulate, but a **positive** Eu anomaly is not necessary to define a cumulate (Wolff et al., 2020). Extensive plagioclase fractionation in mafic to intermediate magmas can be a potential process leading to a significant negative Eu anomaly in dacitic to rhyolitic magmas; hence, the initial conditions of magmas intruding upper crustal reservoirs present already a negative Eu anomaly, and feldspar accumulation may not be enough to fully compensate for this initial deficit in Eu (Hunter, 1998; Deering and Bachmann, 2010; Wolff et al., 2020). Another process which can suppress a positive Eu anomaly is the accumulation of ferromagnesian phases in a cumulate, which usually have particularly low Eu concentrations, prohibiting a potential overturn of the Eu anomaly from negative to positive.

Evidence From Pre-eruptive Reservoir Conditions

Pre-eruptive magmatic temperatures, water contents and pressures presented above broadly overlap between (rhyo-) dacitic melt cap and cumulate mush, indicating strong chemical and physical links between the melts present in early-erupted, silicic pumices and late-erupted scoria. The tendency toward slightly increased temperatures and pressures observed in the cumulate mush, outlined by the Al increase toward the rims of some amphiboles, can be explained by the injection of andesitic to dacitic recharge magmas at the base of the reservoir prior to eruption, providing heat to reactivate the cumulate mush from below, and initiate cumulate remelting. Those findings underline the genetic relation between melts present in crystal-poor, silicic and crystal-rich, more mafic units.

Evidence for Cumulate Rejuvenation

Magma recharge (should it be mafic or intermediate in composition) provides heat to an upper crustal reservoir, typically able to trigger partial remelting of pre-existing crystalline material ("rejuvenation"). In large reservoirs, however, single recharge events are potentially small enough in volume to prevent a significant shift of magma compositions (Wolff et al., 2015). Hence, distinguishing between effects of recharge and products of cumulate melting must rely on petrologic evidence (e.g., Wolff et al., 2020). Such evidence might be given by enrichment of elements (compatible in certain low temperature phases) like Ba, Ti, Eu and Sr in groundmass glasses and recrystallization rims revealing preceding recharge-induced cumulate rejuvenation (Hildreth and Wilson, 2007; Bachmann et al., 2014; Wolff et al., 2015; Forni et al., 2016; D'Oriano et al., 2017; Sliwinski et al., 2019). Hot recharge entering into the cumulate mush initiates (partial) melting of low temperature phases (e.g., alkali feldspar, biotite, low-An plagioclase) leading to local enrichment of the respective compatible elements in the surrounding melts. Recrystallization of mineral rims from those melts will then record amplified concentrations in those elements. The Aso system, however, is rather dominated by refractory minerals such as pyroxene and amphibole. Hence, cumulate melting signatures are expected to be less pronounced than in more fusible systems, such as the Carpenter Ridge Tuff (Bachmann et al., 2014) or the Campanian Ignimbrite (Forni et al., 2016). Nevertheless, recharge-induced cumulate melting signatures in the Aso system are given by.

(1) Sr enrichment in rims of late-erupted plagioclases tracing local enrichment of Sr within the melt prior to the crystallization of the rims (**Figure 5D**),
(2) Variations in Eu anomaly in groundmass glasses from deeply negative to slightly positive (**Figure 2E**),
(3) The presence of mafic minerals (high-Mg# clinopyroxenes and rare olivine, **Figures 4A,C**,**5A,B**),
(4) Reverse and oscillatory zoning in crystals (amphibole, plagioclase and clinopyroxene) predominantly found in late-erupted crystal-rich clasts (**Figure 7**).

Enrichment of Sr and Eu in plagioclase rims and groundmass glasses in Aso-4 samples is interpreted to be the result of recharge-induced melting of low-An plagioclases comprising high concentrations of both elements. This hypothesis is strengthened by the sieved structure displayed by plagioclase cores in late-erupted scoria, which may result from (partial) remelting. The presence of mafic minerals as well as reverse and oscillatory zoning of minerals such as amphibole (**Figure 7**) further record entering of recharge into the system prior to eruption. Substitution mechanisms controlling amphibole chemistry are strongly affected by temperature and pressure variations within the reservoir and also appear to be sensitive to changes in melt chemistry (Bachmann and Dungan, 2002; Zhang et al., 2017). Three main substitutions influence the chemistry of Aso-4 amphiboles 1) the temperature-sensitive Ti-Tschermak exchange ($^{T}Si + {}^{B}Mn = {}^{IV}Al + {}^{C}Ti$; **Figure 6A**), 2) the temperature-sensitive Edenite-exchange, ($^{A}\square + {}^{T}Si = {}^{A}(Na+K) + {}^{IV}Al$; **Figure 6B**), and 3) the pressure-sensitive Al-Tschermak exchange ($^{T}Si + {}^{C}(Mg+Fe) = {}^{IV}Al + {}^{VI}Al$; **Figure 6C**). All substitutions show slightly positive correlations indicating increase of temperature and pressure or changing melt composition throughout amphibole crystallization. The non-linear behavior observed for the Ti-Tschermak substitution (**Figure 6A**) might be caused by additional temperature effects. Furthermore, a large number of core-to-rim profiles measured in amphibole record rimward increase of Al^{IV}, $(Na + K)^{A}$ and Al^{VI} concomitant with decrease of SiO_2, Ti and Mn possibly related to the Edenite-exchange and the Al-Tschermak substitution. This likewise suggests increasing temperature and pressure throughout amphibole crystallization likely caused by entering of hot, intermediate recharge into the reservoir. The observed changes might also be affected by variations in melt composition which might again be induced by mafic recharge.

Petrogenetic Model of the Pre-aso 4 Magmatic System and Concluding Remarks

Based on the above-mentioned observations, we suggest that *magma mixing is not the main factor driving the generation of the zoned ignimbrite, although it played a significant role in*

reactivating the reservoir prior to eruption, allowing for the evacuation of crystal-rich cumulate portions. Hence, a refined model for the generation of the large zoned ignimbrite is elaborated. Key for this newly extended model is melt extraction from a high-crystallinity reservoir ("crystal mush"), leaving behind complementary cumulates in the upper crust, which became remobilized prior to eruption by hot recharge entering the reservoir inducing local, small-scale magma mixing.

During incremental growth of the (rhyo-)dacitic magma reservoir in the upper crust (fed by andesitic-dacitic recharge), magma was mostly stored as a high-crystallinity mush (Koyaguchi and Kaneko, 1999; Marsh, 2004; Parmigiani et al., 2014; Karakas et al., 2017; Szymanowski et al., 2019). Extraction of interstitial melts of (rhyo-) dacitic composition then led to the formation of a crystal-poor melt cap at the top of the reservoir, leaving behind a complementary cumulate below. Hot, less evolved recharge entering at the base of the reservoir prior to eruption initiated cumulate melting and local, small-scale magma mixing, thereby lowering the crystallinity of the cumulate, ultimately allowing portions of it to erupt. The melt-rich cap of (rhyo-)dacitic composition was erupted early during the caldera-forming event producing crystal-poor, silicic units, while late-erupted, crystal-rich units of more mafic bulk composition are interpreted to be erupted cumulate. Similar observations made in other volcanic units like Crater Lake (Bacon and Druitt, 1988), Ammonia Tanks Tuff (Deering et al., 2011), Carpenter Ridge Tuff (Bachmann et al., 2014; Wolff et al., 2015), Gaviotas, Enramada, Adeje, Arico and El Abrigo formations (Sliwinski et al., 2015), Campanian Ignimbrite (Forni et al., 2016), Lajes Ignimbrite (D'Oriano et al., 2017), and Peach Spring Tuff (Foley et al., 2020) imply that the model presented here is applicable not only for Aso but provides a reasonable model for the formation of numerous zoned ignimbrites around the world.

DATA AVAILABILITY STATEMENT

The original contributions presented in the study are included in the article/**Supplementary Material**, further inquiries can be directed to the corresponding author.

AUTHOR CONTRIBUTIONS

Fieldwork was performed by FK, OB, NG and AM. Data collection was conducted by FK and NG. The manuscript was prepared by FK with the help of OB, NG and AM. All authors contributed to data evaluation and interpretation.

ACKNOWLEDGMENTS

We would like to thank Julien Allaz and Julia Neukampf for their helpful assistance during microprobe measurements. Furthermore, we would like to express our gratitude to Marcel Guillong and Peter Tollan for their great assistance during laser analysis. The authors thank reviewers V. C. Smith and C. Barnes, whose comments significantly improved the quality of the manuscript, and editor M. Stock for careful handling of the manuscript.

SUPPLEMENTARY MATERIAL

The Supplementary Material for this article can be found online at: https://www.frontiersin.org/articles/10.3389/feart.2020.614267/full#supplementary-material.

REFERENCES

Albert, P. G., Smith, V. C., Suzuki, T., McLean, D., Tomlinson, E. L., Miyabuchi, Y., et al. (2019). Geochemical characterisation of the Late Quaternary widespread Japanese tephrostratigraphic markers and correlations to the Lake Suigetsu sedimentary archive (SG06 core). *Quat. Geochronol.* 52, 103–131. doi:10.1016/j.quageo.2019.01.005

Anderson, J. L., and Smith, D. R. (1995). The effects of temperature and fO_2 on the Al-in-hornblende barometer. *Amer. Mineral.* 80 (5-6), 545–559. doi:10.2138/am-1995-5-615

Aoki, K. (2008). Revised age and distribution of ca. 87 ka Aso-4 tephra based on new evidence from the northwest Pacific Ocean. *Quat. Int.* 178 (1), 100–118. doi:10.1016/j.quaint.2007.02.005

Bachmann, O., and Bergantz, G. W. (2004). On the origin of crystal-poor rhyolites: extracted from batholithic crystal mushes. *J. Petrol.* 45 (8), 1565–1582. doi:10.1093/petrology/egh019

Bachmann, O., Deering, C. D., Lipman, P. W., and Plummer, C. (2014). Building zoned ignimbrites by recycling silicic cumulates: insight from the 1,000 km^3 Carpenter Ridge Tuff, CO. *Contrib. Mineral. Petrol.* 167 (6), 1025. doi:10.1007/s00410-014-1025-3

Bachmann, O., Deering, C. D., Ruprecht, J. S., Huber, C., Skopelitis, A., and Schnyder, C. (2012). Evolution of silicic magmas in the Kos-Nisyros volcanic center, Greece: a petrological cycle associated with caldera collapse. *Contrib. Mineral. Petrol.* 163 (1), 151–166. doi:10.1007/s00410-011-0663-y

Bachmann, O., and Dungan, M. A. (2002). Temperature-induced Al-zoning in hornblendes of the fish canyon magma, Colorado. *Am. Mineral.* 87 (8–9), 1062–1076. doi:10.2138/am-2002-8-903

Bachmann, O., and Huber, C. (2016). Silicic magma reservoirs in the Earth's crust. *Am. Mineral.* 101 (11), 2377–2404. doi:10.2138/am-2016-5675

Bachmann, O., and Huber, C. (2019). The inner workings of crustal distillation columns; the physical mechanisms and rates controlling phase separation in silicic magma reservoirs. *J. Petrol.* 60 (1), 3–18. doi:10.1093/petrology/egy103

Bacon, C. R., and Druitt, T. H. (1988). Compositional evolution of the zoned calcalkaline magma chamber of Mount Mazama, Crater Lake, Oregon. *Contrib. Mineral. Petrol.* 98 (2), 224–256. doi:10.1007/bf00402114

Barnes, C. G., Coint, N., and Yoshinobu, A. (2016). Crystal accumulation in a tilted arc batholith. *Am. Mineral.* 101 (8), 1719–1734. doi:10.2138/am-2016-5404

Beane, R., and Wiebe, R. A. (2012). Origin of quartz clusters in Vinalhaven granite and porphyry, coastal Maine. *Contrib. Mineral. Petrol.* 163 (6), 1069–1082. doi:10.1007/s00410-011-0717-1

Boehnke, P., Bruce Watson, E., Trail, D., Mark Harrison, T., and Schmitt, A. K. (2013). Zircon saturation re-revisited. *Chem. Geol.* 351, 324–334. doi:10.1016/j.chemgeo.2013.05.028

De Maisonneuve, C. B., and Bergal-Kuvikas, O. (2020). Timing, magnitude and geochemistry of major Southeast Asian volcanic eruptions: identifying tephrochronologic markers. *J. Quat. Sci.* 35 (1–2), 272–287. doi:10.1002/jqs.3181

Deering, C. D., and Bachmann, O. (2010). Trace element indicators of crystal accumulation in silicic igneous rocks. *Earth Planet Sci. Lett.* 297 (1–2), 324–331. doi:10.1016/j.epsl.2010.06.034

Deering, C. D., Bachmann, O., and Vogel, T. A. (2011). The Ammonia Tanks Tuff: erupting a melt-rich rhyolite cap and its remobilized crystal cumulate. *Earth Planet Sci. Lett.* 310 (3–4), 518–525. doi:10.1016/j.epsl.2011.08.032

D'Oriano, C., Landi, P., Pimentel, A., and Zanon, V. (2017). Magmatic processes revealed by anorthoclase textures and trace element modeling: The case of the Lajes Ignimbrite eruption (Terceira Island, Azores). *J. Volcanol. Geother. Res.* 344, 44–63. doi:10.1016/j.jvolgeores.2017.08.012

Dunbar, N. W., Kyle, P. R., and Wilson, C. J. N. (1989). Evidence for limited zonation in silicic magma systems, Taupo Volcanic Zone, New Zealand. *Geology.* 17 (3), 234–236. doi:10.1130/0091-7613(1989)017<0234:EFLZIS>2.3.CO;2

Eichelberger, J. C., Chertkoff, D. G., Dreher, S. T., and Nye, C. J. (2000). Magmas in collision: rethinking chemical zonation in silicic magmas. *Geology.* 28 (7), 603–606. doi:10.1130/0091-7613(2000)028<0603:MICRCZ>2.3.CO;2

Ellis, B. S., Bachmann, O., and Wolff, J. A. (2014). Cumulate fragments in silicic ignimbrites: the case of the Snake River Plain. *Geology* 42 (5), 431–434. doi:10.1130/G35399.1

Ellis, B. S., and Wolff, J. A. (2012). Complex storage of rhyolite in the central snake river plain. *J. Volcanol. Geoth. Res.* 211–212, 1–11. doi:10.1016/j.jvolgeores.2011.10.002

Evans, B. W., and Bachmann, O. (2013). Implications of equilibrium and disequilibrium among crystal phases in the Bishop Tuff. *Am. Mineral.* 98 (1), 271–274. doi:10.2138/am.2013.4280

Fiedrich, A. M., Bachmann, O., Ulmer, P., Deering, C. D., Kunze, K., and Leuthold, J. (2017). Mineralogical, geochemical, and textural indicators of crystal accumulation in the Adamello Batholith (Northern Italy). *Am. Mineral.* 102 (12), 2467–2483. doi:10.2138/am-2017-6026

Foley, M. L., Miller, C. F., and Gualda, G. A. R. (2020). Architecture of a super-sized magma chamber and remobilization of its basal cumulate (Peach spring tuff, USA). *J. Petrol.* 61 (1), egaa020. doi:10.1093/petrology/egaa020

Forni, F., Bachmann, O., Mollo, S., De Astis, G., Gelman, S. E., and Ellis, B. S. (2016). The origin of a zoned ignimbrite: insights into the Campanian Ignimbrite magma chamber (Campi Flegrei, Italy). *Earth Planet Sci. Lett.* 449, 259–271. doi:10.1016/j.epsl.2016.06.003

Gelman, S. E., Deering, C. D., Bachmann, O., Huber, C., and Gutiérrez, F. J. (2014). Identifying the crystal graveyards remaining after large silicic eruptions. *Earth Planet. Sci. Let.* 403, 299–306. doi:10.1016/j.epsl.2014.07.005

Geshi, N. (2020). Volcanological challenges to understanding explosive large-scale eruptions. *Earth Planets Space.* 72 (1), 1–10. doi:10.1186/s40623-020-01222-1

Graeter, K. A., Beane, R. J., Deering, C. D., Gravley, D., and Bachmann, O. (2015). Formation of rhyolite at the Okataina Volcanic Complex, New Zealand: new insights from analysis of quartz clusters in plutonic lithics. *Am. Mineral.* 100 (8–9), 1778–1789. doi:10.2138/am-2015-5135

Guillong, M., Meier, D. L., Allan, M. M., Heinrich, C. A., and Yardley, B. W. D. (2008). SILLS: a matlab-based program for the reduction of laser ablation ICP–MS data of homogeneous materials and inclusions. *Mineralog. Assoc. Can. Short Course* 40, 328–333.

Hervig, R. L., and Dunbar, N. W. (1992). Cause of chemical zoning in the Bishop (California) and Bandelier (New Mexico) magma chambers. *Earth Planet Sci. Lett.* 111 (1), 97–108. doi:10.1016/0012-821X(92)90172-R

Hildreth, W. (1981). Gradients in silicic magma chambers: implications for lithospheric magmatism. *J. Geophys. Res. Solid Earth* 86 (B11), 10153–10192. doi:10.1029/jb086ib11p10153

Hildreth, W. (2004). Volcanological perspectives on long valley, mammoth mountain, and mono craters: several contiguous but discrete systems. *J. Volcanol. Geoth. Res.* 136 (3–4), 169–198. doi:10.1016/j.jvolgeores.2004.05.019

Hildreth, W., and Wilson, C. J. N. (2007). Compositional zoning of the bishop tuff. *J. Petrol.* 48 (5), 951–999. doi:10.1093/petrology/egm007

Holland, T., and Blundy, J. (1994). Non-ideal interactions in calcic amphiboles and their bearing on amphibole-plagioclase thermometry. *Contrib. Mineral. Petrol.* 116 (4), 433–447. doi:10.1007/BF00310910

Holness, M. B., Stock, M. J., and Geist, D. (2019). Magma chambers versus mush zones: Constraining the architecture of sub-volcanic plumbing systems from microstructural analysis of crystalline enclaves. *Philos. Trans. Roy. Soc. A.* 377 (2139). doi:10.1098/rsta.2018.0006

Huber, C., Townsend, M., Degruyter, W., and Bachmann, O. (2019). Optimal depth of subvolcanic magma chamber growth controlled by volatiles and crust rheology. *Nat. Geosci.* 12 (9), 762–768. doi:10.1038/s41561-019-0415-6

Humphreys, M. C. S., Cooper, G. F., Zhang, J., Loewen, M., Kent, A. J. R., Macpherson, C. G., et al. (2019). Unravelling the complexity of magma plumbing at Mount St. Helens: a new trace element partitioning scheme for amphibole. *Contrib. Mineral. Petrol.* 174 (1), 1–15. doi:10.1007/s00410-018-1543-5

Hunter, A. G. (1998). Intracrustal controls on the coexistence of tholeiitic and calc-alkaline magma series at Aso Volcano, SW Japan. *J. Petrol.* 39 (7), 1255–1284. doi:10.1093/petroj/39.7.1255

Ishibashi, H., Suwa, Y., Miyoshi, M., Yasuda, A., and Hokanishi, N. (2018). Amphibole–melt disequilibrium in silicic melt of the Aso-4 caldera-forming eruption at Aso Volcano, SW Japan. *Earth Planets Space* 70 (1), 137. doi:10.1186/s40623-018-0907-4

Kaneko, K., Kamata, H., Koyaguchi, T., Yoshikawa, M., and Furukawa, K. (2007). Repeated large-scale eruptions from a single compositionally stratified magma chamber: an example from Aso volcano, Southwest Japan. *J. Volcanol. Geoth. Res.* 167 (1–4), 160–180. doi:10.1016/j.jvolgeores.2007.05.002

Karakas, O., Degruyter, W., Bachmann, O., and Dufek, J. (2017). Lifetime and size of shallow magma bodies controlled by crustal-scale magmatism. *Nat. Geosci.* 10 (6), 446–450. doi:10.1038/ngeo2959

Kelemen, P. B., Hanghøj, K., and Greene, A. R. (2003). One view of the geochemistry of subduction-related magmatic arcs, with an emphasis on primitive andesite and lower crust. Treatise Geochem. 3, 659. doi:10.1016/B0-08-043751-6/03035-8

Kiss, B., Harangi, S., Ntaflos, T., Mason, P. R. D., and Pál-Molnár, E. (2014). Amphibole perspective to unravel pre-eruptive processes and conditions in volcanic plumbing systems beneath intermediate arc volcanoes: a case study from Ciomadul volcano (SE Carpathians). *Contrib. Mineral. Petrol.* 167 (3), 1–27. doi:10.1007/s00410-014-0986-6

Koyaguchi, T., and Kaneko, K. (1999). A two-stage thermal evolution model of magmas in continental crust. *J. Petrol.* 40 (2), 241–254. doi:10.1093/petroj/40.2.241

Lee, C. T. A., and Bachmann, O. (2014). How important is the role of crystal fractionation in making intermediate magmas? Insights from Zr and P systematics. *Earth Planet. Sci. Lett.* 393, 266–274. doi:10.1016/j.epsl.2014.02.044

Lipman, PW. (2006). Chemical analyses of tertiary volcanic rocks, central San Juan Caldera complex, southwestern Colorado. US Department of the Interior, US Geological Survey, Open-File Report 2004–1194. doi:10.3133/ofr20041194

Lipman, P. W. (1967). Mineral and chemical variations within an ash-flow sheet from Aso caldera, Southwestern Japan. *Contrib. Mineral. Petrol.* 16 (4), 300–327. doi:10.1007/BF00371528

Lubbers, J., Deering, C., and Bachmann, O. (2020). Genesis of rhyolitic melts in the upper crust: Fractionation and remobilization of an intermediate cumulate at Lake City caldera, Colorado, USA. *J. Volcanol. Geotherm. Res.* 392, 106750. doi:10.1016/j.jvolgeores.2019.106750

Machida, H., and Arai, F. (1983). Extensive ash falls in and around the sea of Japan from large late quaternary eruptions. *J. Volcanol. Geoth. Res.* 18 (1-4), 151–164. doi:10.1016/0377-0273(83)90007-0

Machida, H. (2002). Volcanoes and tephras in the Japan area. *Global Environ. Res.* 6, 19–28. Available at: http://www.airies.or.jp/attach.php/6a6f75726e616c5f30362d32656e67/save/0/0/06_2-03.pdf.

Marsh, B. (2004). A magmatic mush column rosetta stone: the Mcmurdo dry valleys of Antarctica. *Eos Transact. Am. Geophys. Union* 85 (47), 497. doi:10.1029/2004EO470001

Matsumoto, T. (1943). The four gigantic caldera volcanoes of Kyushu. *Japanese J. Geol. Geograp.* 19, 1–57. (in Japanese).

McLean, D., Albert, P. G., Suzuki, T., Nakagawa, T., Kimura, J.-I., Chang, Q., et al. (2020). Constraints on the timing of explosive volcanism at Aso and Aira calderas (Japan) between 50 and 30 ka: new insights from the Lake Suigetsu sedimentary record (SG14 core). *Geochem. Geophys. Geosys.* 21 (8), 1–21. doi:10.1029/2019gc008874

Meurer, W. P., and Boudreau, A. E. (1998). Compaction of igneous cumulates part II: compaction and the development of igneous foliations. *J. Geol.* 106 (3), 293–304. doi:10.1086/516023

Milner, D. M., Cole, J. W., and Wood, C. P. (2003). Mamaku Ignimbrite: a caldera-forming ignimbrite erupted from a compositionally zoned magma chamber in Taupo Volcanic Zone, New Zealand. *J. Volcanol. Geoth. Res.* 122 (3–4), 243–264. doi:10.1016/S0377-0273(02)00504-8

Miyabuchi, Y. (2009). A 90,000-year tephrostratigraphic framework of Aso volcano, Japan. *Sediment. Geol.* 220 (3–4), 169–189. doi:10.1016/j.sedgeo.2009.04.018

Miyabuchi, Y. (2011). Post-caldera explosive activity inferred from improved 67-30ka tephrostratigraphy at Aso Volcano, Japan. *J. Volcanol. Geoth. Res.* 205 (3–4), 94–113. doi:10.1016/j.jvolgeores.2011.05.004

Miyoshi, M., Sumino, H., Miyabuchi, Y., Shinmura, T., Mori, Y., Hasenaka, T., et al. (2012). K-Ar ages determined for post-caldera volcanic products from Aso volcano, central Kyushu, Japan. *J. Volcanol. Geoth. Res.* 229 (230), 64–73. doi:10.1016/j.jvolgeores.2012.04.003

Morimoto, N. (1988). Nomenclature of pyroxenes. *Mineral. Petrol.* 39 (1), 55–76. doi:10.1007/bf01226262

Newhall, C. G., and Self, S. (1982). The volcanic explosivity index (VEI): an estimate of explosive magnitude for historical volcanism. *J. Geophys. Res.* 87 (C2), 1231–1238. doi:10.1029/jc087ic02p01231

Newhall, C., Self, S., and Robock, A. (2018). Anticipating future volcanic explosivity index (VEI) 7 eruptions and their chilling impacts. *Geosphere* 14 (2), 572–603. doi:10.1130/GES01513.1

Nobile, A., Acocella, V., Ruch, J., Aoki, Y., Borgstrom, S., Siniscalchi, V., et al. (2017). Steady subsidence of a repeatedly erupting caldera through InSAR observations: Aso, Japan. *Bull. Volcanol.* 79 (5). doi:10.1007/s00445-017-1112-1

Pamukcu, A. S., Carley, T. C., Gualda, G. A. R., Miller, C. F., and Ferguson, C. A. (2013). The evolution of the peach spring giantmagma body: Evidence from accessory mineraltextures and compositions, bulk pumice and glass geochemistry, and rhyolite-MELTS modeling. *J. Petrology.* 54 (6), 1109–1148. doi:10.1093/petrology/egt007

Papale, P., and Marzocchi, W. (2019). Volcanic threats to global society. *Science* 363 (6433), 1275–1276. doi:10.1126/science.aaw7201

Parmigiani, A., Huber, C., and Bachmann, O. (2014). Mush microphysics and the reactivation of crystal-rich magma reservoirs. *J. Geophys. Res. Solid Earth* 119 (8), 6308–6322. doi:10.1002/2014JB011124

Paton, C., Hellstrom, J., Paul, B., Woodhead, J., and Hergt, J. (2011). Iolite: freeware for the visualisation and processing of mass spectrometric data. *J. Anal. Atomic Spectrom* 26 (12), 2508–2518. doi:10.1039/c1ja10172b

Peccerillo, A., and Taylor, S. R. (1976). Geochemistry of Eocene calc-alkaline volcanic rocks from the Kastamonu area, northern Turkey. *Contrib. Mineral. Petrol.* 58 (1), 63–81. doi:10.1007/bf00384745

Piccoli, P. M., and Candela, P. A. (2019). Apatite in igneous systems. *Phosphates Geochem. Geobiol. Mater. Import* 48, 255–292. doi:10.2138/rmg.2002.48.6

Popa, R. G., Bachmann, O., Ellis, B. S., Degruyter, W., Tollan, P., and Kyriakopoulos, K. (2019). A connection between magma chamber processes and eruptive styles revealed at Nisyros-Yali volcano (Greece). *J. Volcanol. Geoth. Res.* 387, 106666. doi:10.1016/j.jvolgeores.2019.106666

Popa, R. G., Dietrich, V. J., and Bachmann, O. (2020). Effusive-explosive transitions of water-undersaturated magmas. The case study of methana volcano, south aegean arc. *J. Volcanol. Geoth. Res.* 399, 106884. doi:10.1016/j.jvolgeores.2020.106884

Putirka, K. (2016). Amphibole thermometers and barometers for igneous systems and some implications for eruption mechanisms of felsic magmas at arc volcanoes. *Amer. Mineral.* 101 (4), 841–858. doi:10.2138/am-2016-5506

Putirka, K. D. (2008). Thermometers and barometers for volcanic systems. *Rev. Mineral. Geochem.* 69, 61–120. doi:10.2138/rmg.2008.69.3

Rollinson, HR (1993). Using geochemical data: evaluation, presentation and interpretation. Harlow: Pearson Education Limited.

Rowe, M. C., Ellis, B. S., and Lindeberg, A. (2012). Quantifying crystallization and devitrifcation of rhyolites by means of X-ray diffraction and electron microprobe analysis. *Am. Mineral.* 97 (10), 1685–1699. doi:10.2138/am.2012.4006

Self, S. (2015). Explosive super-eruptions and potential global impacts. *Volcanic Hazards Risks Disasters.* 399–418. doi:10.1016/B978-0-12-396453-3.00016-2

Self, S. (2006). The effects and consequences of very large explosive volcanic eruptions. *Phil. Trans. Math. Phys. Eng. Sci.* 364 (1845), 2073–2097. doi:10.1098/rsta.2006.1814

Sliwinski, J., Bachmann, O., Ellis, B. S., Dávila-Harris, P., Nelson, B. K., and Dufek, J. (2015). Eruption of shallow crystal cumulates during explosive phonolitic eruptions on Tenerife, Canary Islands. *J. Petrolog.* 56 (11), 2173–2194. doi:10.1093/petrology/egv068

Sliwinski, J., Farsky, D., Lipman, P. W., Guillong, M., and Bachmann, O. (2019). Rapid magma generation or shared magmatic reservoir? Petrology and geochronology of the rat creek and nelson mountain tuffs, CO, USA. *Front. Earth Sci.* 7, 271. doi:10.3389/feart.2019.00271

Sun, S. S., and McDonough, W. F. (1989). Chemical and isotopic systematics of oceanic basalts: Implications for mantle composition and processes. *Geol. Soc. Special Pub.* 42, 313–345. doi:10.1144/GSL.SP.1989.042.01.19

Szymanowski, D., Ellis, B. S., Wotzlaw, J. F., and Bachmann, O. (2019). Maturation and rejuvenation of a silicic magma reservoir: high-resolution chronology of the Kneeling Nun Tuff. *Earth Planet Sci. Lett.* 510, 103–115. doi:10.1016/j.epsl.2019.01.007

Takarada, S., and Hoshizumi, H. (2020). Distribution and eruptive volume of aso-4 pyroclastic density current and tephra fall deposits, Japan: a M8 super-eruption. *Front. Earth Sci.* 8, 170. doi:10.3389/feart.2020.00170

Togashi, S., Imai, N., Okuyama-Kusunose, Y., Tanaka, T., Okai, T., Koma, T., et al. (2000). Young upper crustal chemical composition of the orogenic Japan Arc. *Geochem. Geophys. Geosyst.* 1 (11), 1049. doi:10.1029/2000GC000083

Tsuji, T., Ikeda, M., Furusawa, A., Nakamura, C., Ichikawa, K., Yanagida, M., et al. (2018). High resolution record of Quaternary explosive volcanism recorded in fluvio-lacustrine sediments of the Uwa basin, southwest Japan. *Quat. Int.* 471, 278–297. doi:10.1016/j.quaint.2017.10.016

Ushioda, M., Miyagi, I., Suzuki, T., Takahashi, E., and Hoshizumi, H. (2020). Preeruptive P-T conditions and H2O concentration of the aso-4 silicic end-member magma based on high-pressure experiments. *J. Geophys. Res. Solid Earth* 125 (3), e2019JB018481. doi:10.1029/2019JB018481

Waters, L. E., and Lange, R. A. (2015). An updated calibration of the plagioclase-liquid hygrometer-thermometer applicable to basalts through rhyolites. *Am. Mineral.* 100 (10), 2172–2184. doi:10.2138/am-2015-5232

Watson, E. B., and Harrison, T. M. (1983). Zircon saturation revisited: temperature and composition effects in a variety of crustal magma types. *Earth Planet Sci. Lett.* 64 (2), 295–304. doi:10.1016/0012-821X(83)90211-X

Watts, K. E., John, D. A., Colgan, J. P., Henry, C. D., Bindeman, I. N., and Schmitt, A. K. (2016). Probing the volcanic-plutonic connection and the genesis of crystal-rich rhyolite in a deeply dissected supervolcano in the Nevada Great Basin: Source of the late Eocene Caetano Tuff. *J. Petrology.* 8 (57), 1599–1644. doi:10.1093/petrology/egw051

Williams, H. (1942). *The geology of Crater Lake national park, Oregon: with a reconnaissance of the cascade range southward to mount Shasta.* Washington, D.C., United States: Carnegie institution.

Wolff, J. A., Ellis, B. S., Ramos, F. C., Starkel, W. A., Boroughs, S., Olin, P. H., et al. (2015). Remelting of cumulates as a process for producing chemical zoning in silicic tuffs: a comparison of cool, wet and hot, dry rhyolitic magma systems. *Lithos.* 236–237, 275–286. doi:10.1016/j.lithos.2015.09.002

Wolff, J. A., Forni, F., Ellis, B. S., and Szymanowski, D. (2020). Europium and barium enrichments in compositionally zoned felsic tuffs: a smoking gun for the origin of chemical and physical gradients by cumulate melting. *Earth Planet Sci. Lett.* 540, 116251. doi:10.1016/j.epsl.2020.116251

Wolff, J. A., Ramos, F. C., and Davidson, J. P. (1999). Sr isotope disequilibrium during differentiation of the Bandelier Tuff: constraints on the crystallization of a large rhyolitic magma chamber. *Geology* 27 (6), 495–498. doi:10.1130/0091-7613(1999)027<0495:SIDDDO>2.3.CO;2

Wörner, G., and Schmincke, H.-U. (1984). Mineralogical and chemical zonation of the laacher see tephra sequence (east eifel, W. Germany). *J. Petrol.* 25 (4), 805–835. doi:10.1093/petrology/25.4.805

Žák, J., Paterson, S. R., and Memeti, V. (2007). Four magmatic fabrics in the Tuolumne batholith, central Sierra Nevada, California (USA): implications for interpreting fabric patterns in plutons and evolution of magma chambers in the upper crust. *Geol. Soc. Am. Bull.* 119 (1–2), 184–201. doi:10.1130/B25773.1

Zhang, J., Humphreys, M. C. S., Cooper, G. F., Davidson, J. P., and Macpherson, C. G. (2017). Magma mush chemistry at subduction zones, revealed by new melt major element inversion from calcic amphiboles. *Am. Mineral.* 102 (6), 1353–1367. doi:10.2138/am-2017-5928

Conflict of Interest: The authors declare that the research was conducted in the absence of any commercial or financial relationships that could be construed as a potential conflict of interest.